

# CrystEngComm

Accepted Manuscript



This is an *Accepted Manuscript*, which has been through the Royal Society of Chemistry peer review process and has been accepted for publication.

*Accepted Manuscripts* are published online shortly after acceptance, before technical editing, formatting and proof reading. Using this free service, authors can make their results available to the community, in citable form, before we publish the edited article. We will replace this *Accepted Manuscript* with the edited and formatted *Advance Article* as soon as it is available.

You can find more information about *Accepted Manuscripts* in the [Information for Authors](#).

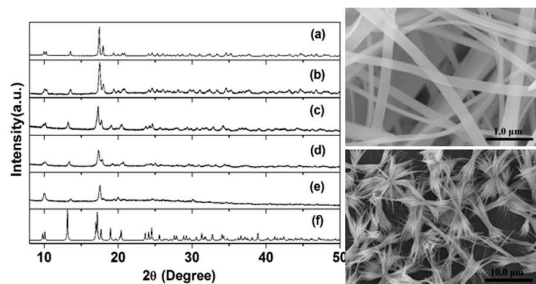
Please note that technical editing may introduce minor changes to the text and/or graphics, which may alter content. The journal's standard [Terms & Conditions](#) and the [Ethical guidelines](#) still apply. In no event shall the Royal Society of Chemistry be held responsible for any errors or omissions in this *Accepted Manuscript* or any consequences arising from the use of any information it contains.

---

## A series of nano/micro-sized metal-organic frameworks with tunable photoluminescence properties

Yuhua Zheng, Kai Liu, Xunsun, Rengui Guan, Huijuan Su, Hongpeng You<sup>\*</sup>, Caixia Qi<sup>\*</sup>

*CrystEngComm*, xxxx, xx, xxxx



Hierarchically assembled nanostructures of lanthanide-based MOFs with tunable emissions have been successfully fabricated via a simple method at room temperature.

# A series of nano/micro-sized metal-organic frameworks with tunable photoluminescence properties

Yuhua Zheng,<sup>a</sup> Kai Liu,<sup>b</sup> Xun Sun,<sup>a</sup> Rengui Guan,<sup>a</sup> Huijuan Su,<sup>a</sup> Hongpeng You,<sup>c\*</sup> Caixia Qi<sup>a\*</sup>

<sup>a</sup>Shandong Applied Research Center for Gold Nanotechnology (Au-SDARC), School of Chemistry and Chemical Engineering, Yantai University, Yantai 264005, PR China.

<sup>b</sup>Department of Polymer Chemistry, Zernike Institute for Advanced Materials, University of Groningen, Nijenborgh 4, 9747 AG Groningen, The Netherlands.

<sup>c</sup>State Key Laboratory of Rare Earth Resource Utilization, Changchun Institute of Applied Chemistry, Chinese Academy of Sciences, Changchun 130022, PR China.

\* Corresponding author. Email: hpyou@ciac.ac.cn; qicx@ytu.edu.cn

## Abstract

Present studies on metal-organic frameworks (MOF) mainly focus on macro-scaled single crystals. However, the realization of MOF nanocrystals via bottom-up one-step method still remains a significant challenge. Here, hierarchically assembled nanostructures of lanthanide-based MOFs with 1D and 3D morphologies have been successfully fabricated via a simple and rapid solution phase method at room temperature. Upon UV excitation, these nanomaterials exhibit highly efficient tunable luminescence properties, which comes from the  $\text{Eu}^{3+}$  or  $\text{Tb}^{3+}$  ions. Moreover, white-light emission can be approached by co-activating the organic ligand,  $\text{Eu}^{3+}$  and  $\text{Tb}^{3+}$  ions in the nano-MOFs.

## 1. Introduction

Metal-organic frameworks (MOFs), in which metal ions or metal clusters are connected by molecular building blocks consisting of organic molecules or organometallic complexes, have attracted a great deal of attention<sup>1-4</sup> due to their well-defined coordination geometries and useful applications in gas storage, catalysis, optics, recognition, and separation. In the past two decades, a structural study of macro-scaled crystalline samples is a main fundamental interest in metal-organic materials based on single-crystal X-ray analysis. However, miniaturizing the size of MOFs crystals to the nanometer scale by functionalizing the crystal interfaces will provide further opportunities to integrate novel functions into the materials without changing the characteristic features of the metal-organic crystal itself, and will allow the correlation between the chemical and physical properties and interfacial structures of

nanocrystalline MOFs (nano-MOF) to be investigated. Recently, several nano- and micro-scaled particles from metal–organic complexes have been successfully prepared by solvent-induced precipitation,<sup>5</sup> reverse microemulsion,<sup>6</sup> electrospinning,<sup>7</sup> hydrothermal,<sup>8</sup> and solvothermal methods.<sup>9</sup> These thought-provoking works suggest that the suitable design of reaction routes and selection of the metal ions and ligands could open a new field for preparing nano/micro-scaled metal–organic materials from the molecular level, enabling their use in a broad range of applications<sup>10-15</sup> including catalysis, biosensing, biomedical imaging, and anticancer drug delivery. However, the introduction of high temperature or pressure for the fabrication of nanoarchitectures induces heterogeneous impurities, increases the production cost, and leads to difficulty for scale-up production.

Lanthanide-based MOFs have been extensively investigated acting as luminescent devices, magnets, catalysts, and other functional materials because of their electronic, optical, and chemical characteristics resulting from the 4f electronic shells.<sup>16-21</sup> In our previous work, some nano-sized metal-organic compounds based on lanthanide ions ( $\text{Ln}^{3+}$ ) and benzenetricarboxylic acid (BTC) have been constructed successfully.<sup>22-25</sup> For example, 1D nanobelt based on the coordinated assembly between the  $\text{Tb}^{3+}$  ions and BTC ligands has been fabricated.<sup>25</sup> The luminescence color of the nanobelts can be easily shifted from green to green-yellow, yellow, orange and red-orange by doping the  $\text{Eu}^{3+}$  ions ( $\text{Tb-BTC:Eu}^{3+}$ ). However, it is a still challenge to develop a general strategy regarding rational choice of different lanthanide ions for tuning nano-MOF assemblies. Moreover, the selection of suitable host-activators and precise control of different combinations of doped  $\text{Ln}^{3+}$  ions are consistently needed for highly efficient tunable nano-MOF luminescence. Herein, we present the successful preparation of a series of nano-MOFs (Y-BTC, Gd-BTC, Ce-BTC, Sm-BTC, and Tm-BTC) with 1D and 3D architectures on a large scale via one-step precipitation in solution phase under ambient conditions (Figure 1). Emission colors are tunable in these nano-MOFs by doping  $\text{Eu}^{3+}$  and  $\text{Tb}^{3+}$  ions. Very interestingly, white light can be approached by the combination of photoluminescence characteristics of BTC ligand and codoped  $\text{Eu}^{3+}$  and  $\text{Tb}^{3+}$  ions in Ce-BTC host.

## 2. Experimental parts

### 2.1 Materials.

The rare earth oxides, including  $\text{Y}_2\text{O}_3$ ,  $\text{Gd}_2\text{O}_3$ ,  $\text{Sm}_2\text{O}_3$ ,  $\text{Tm}_2\text{O}_3$ ,  $\text{Eu}_2\text{O}_3$  and  $\text{Tb}_4\text{O}_7$  (99.99%) were purchased from Wuxi Yiteng Rare-Earth Limited Corporation (China). 1,3,5-

Benzenetricarboxylic acid (BTC) (98%) was purchased from Alfa Aescar Chemical Company. HNO<sub>3</sub> and ethanol (both with purity of A. R.) were purchased from Beijing Fine Chemical Company (China). All of the chemicals were used directly without further purification.

## 2.2 Preparation.

Ln(NO<sub>3</sub>)<sub>3</sub> aqueous solution (pH = 3–4) was obtained by dissolving Y<sub>2</sub>O<sub>3</sub>, Gd<sub>2</sub>O<sub>3</sub>, Sm<sub>2</sub>O<sub>3</sub>, Tm<sub>2</sub>O<sub>3</sub>, Eu<sub>2</sub>O<sub>3</sub> and Tb<sub>4</sub>O<sub>7</sub> in dilute HNO<sub>3</sub> solution under heating with agitation. In a typical synthesis of Tm-BTC/Sm-BTC nanocrystals, 4 mL of 0.5 M Tm(NO<sub>3</sub>)<sub>3</sub> or Sm(NO<sub>3</sub>)<sub>3</sub> aqueous solution was added into 40 mL of 0.05 M BTC ethanol–water solution (v/v = 1:1) under vigorous stirring at room temperature, and a large amount of white precipitate formed. After reaction for 30 min, the precipitate was collected by centrifugation, washed several times with ethanol and water, and dried in air for characterization. A similar process was employed to prepare Gd<sub>0.95</sub>Eu<sub>0.05</sub>-BTC, Gd<sub>0.95</sub>Tb<sub>0.05</sub>-BTC, Ce<sub>0.90</sub>Eu<sub>0.05</sub>Tb<sub>0.05</sub>-BTC, and Y<sub>0.95</sub>Eu<sub>0.05</sub>-BTC, except for adding the mixed Ln(NO<sub>3</sub>)<sub>3</sub> aqueous solutions (e.g., 4 mL of 0.5 M Gd(NO<sub>3</sub>)<sub>3</sub> + 0.21 mL of 0.5 M Eu(NO<sub>3</sub>)<sub>3</sub>) at the initial stage, while other reaction parameters were kept unchanged.

## 2.3 Characterization.

Powder X-ray diffraction (XRD) patterns were performed on a D8 Focus (Bruker) diffractometer (continuous, 40 kV, 40 mA, increment = 0.02°). Thermogravimetric analysis (TGA) data were recorded with a thermal analysis instrument (SDT2960, TA Instruments, New Castle, DE) at the heating rate of 10 °C min<sup>-1</sup> in an air flow of 100 mL·min<sup>-1</sup>. The morphology and composition of the samples were inspected using a field emission scanning electron microscope (FE-SEM, S-4800, Hitachi) equipped with an energy dispersive X-ray spectrum (EDX, JEOL JXA-840). Photoluminescence excitation and emission spectra were recorded with a HitachiF-4500 spectrophotometer equipped with a 150 W xenon lamp as the excitation source.

### 3. Results and discussion

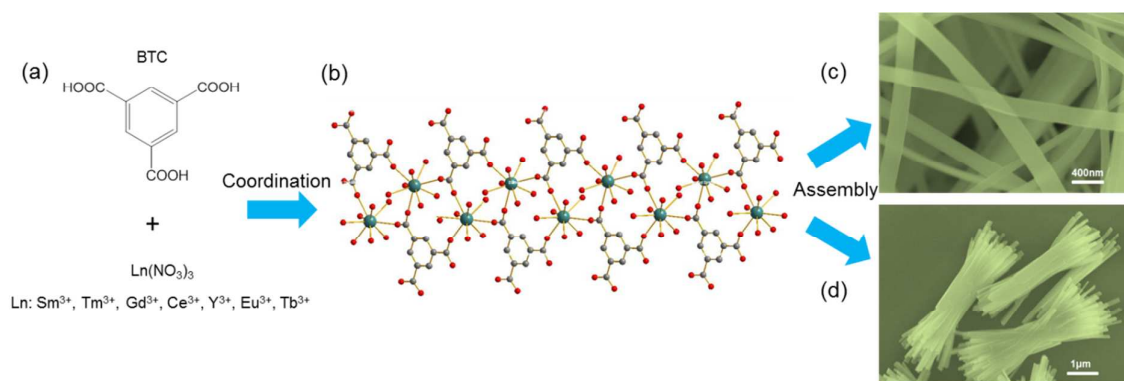


**Figure 1.** Schematic route of preparation of nano/micro-sized crystals of lanthanide benzenetricarboxylate (Ln-BTC). (a) The used building blocks: a series of lanthanide nitrate and organic ligand 1,3,5-benzenetricarboxylic acid. (b) The formed 1D ribbonlike molecular motifs of Ln-BTC (the hydrogen atoms were omitted for clarity, Ln dark green, O red, C gray). (c,d) Coordination induced assembly of Ln-BTC nanocrystals with 1D and 3D architectures.

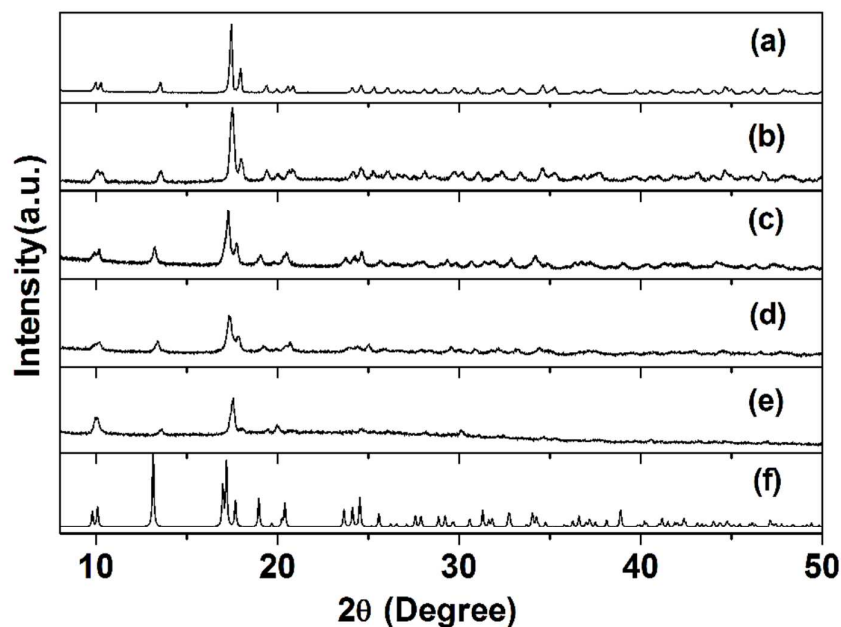


**Figure 2.** XRD patterns of the as-prepared Ln-BTC nanocrystals (a,  $\text{Y}_{0.95}\text{Eu}_{0.05}$ -BTC 1D nanobelt; b,  $\text{Gd}_{0.95}\text{Eu}_{0.05}$ -BTC 1D nanorod; c,  $\text{Ce}_{0.90}\text{Eu}_{0.05}\text{Tb}_{0.05}$ -BTC 3D nanobundles; d, Sm-BTC 3D nanobundles; e, Tm-BTC 3D nanobundles) and simulated XRD pattern using the X-ray structure of La(BTC) single crystal.<sup>26</sup> These results reveal that the obtained samples are

isostructural with the La-BTC structure. The spectral shift of the diffraction peaks can be explained by the change of ionic radii.

Nano-MOFs of Ln-BTC (Sm-BTC, Tm-BTC, Gd<sub>0.95</sub>Eu<sub>0.05</sub>-BTC, Gd<sub>0.95</sub>Tb<sub>0.05</sub>-BTC, Ce<sub>0.90</sub>Eu<sub>0.05</sub>Tb<sub>0.05</sub>-BTC, and Y<sub>0.95</sub>Eu<sub>0.05</sub>-BTC) were prepared by directly mixing Ln(NO<sub>3</sub>)<sub>3</sub> and BTC solutions (Figure 1a). Due to the strong coordinated interactions between the Ln<sup>3+</sup> ions and carboxylic acids of BTC, the formed hydrophobic Ln-BTC was precipitated efficiently from aqueous environment. After centrifugation and dehydration, the purified Ln-BTC samples were firstly analyzed by powder X-ray diffraction (XRD). As shown in Figure 2, all the samples were well-crystallized in spite of the moderate reaction conditions. All of the diffraction peaks can be well indexed to the bulk phase of La-BTC.<sup>26</sup> Their structure can thus be monoclinic, space group *Cc*. No peaks of impurities were detected, indicating that all the Ln<sup>3+</sup> ions have been effectively coordinated with BTC ligand. The center Ln atom is nine-coordinated by three oxygen atoms from three carboxylate groups of BTC ligands as well as six oxygen atoms from water molecules to form a tricapped trigonal prismatic geometry (Figure S1). As shown in Figure 1b, the Ln-BTC MOF structure consists of parallel ribbonlike molecular motifs extending along one direction, which could be the reason for the 1D nanobelt formation (Figure 1c). In addition, the combination of noncovalent interactions (hydrogen-bonding and  $\pi$ - $\pi$  stacking of phenyl groups) could lead to the formation of a 3D network structure (Figure S1), which may benefit for the micro-scaled assembly in 3D directions (Figure 1d). In addition, the spectral shift of the diffraction peaks has been detected (Figure 2), which can be explained by the change of ionic radii. For example, when the La<sup>3+</sup> ions was substituted by the Tm<sup>3+</sup> ions with a smaller radius as a result of lanthanide contraction, the crystal lattice constants as well as d-spacing decreased, and thus the diffraction angles increased accordingly because of the Bragg equation  $\sin \theta = \lambda/2d$ , where *d* is the distance between two crystal planes,  $\theta$  is diffraction angle of an observed peak, and  $\lambda$  is the X-ray wavelength (1.54 Å). Furthermore, thermal behaviors of these samples were investigated by thermal gravimetric analysis (TGA). These TGA curves (Figure S1) exhibited two major stages of rapid weight loss in the temperature range from 80 to 1000°C. The weight loss for the two stages was measured to be ~25 and ~45%, respectively, which is basically in agreement with the theoretical weight loss of the six water molecules (23.68%) and the organic ligand (38.96%) of assumed structure Ln(BTC)(H<sub>2</sub>O)<sub>6</sub>. This indicated that six water molecules are combined in the MOF structure, matching well the structure analysis of bulky La(BTC).<sup>26</sup>



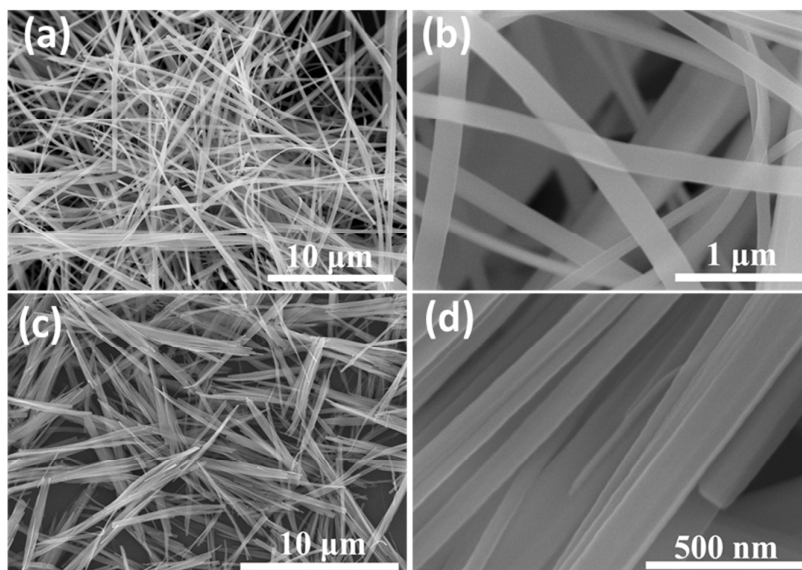


**Figure 3.** SEM images of the Ln-BTC 1D nanocrystals. (a, b) the obtained  $\text{Y}_{0.95}\text{Eu}_{0.05}$ -BTC nanobelt. (c, d) the obtained  $\text{Gd}_{0.95}\text{Eu}_{0.05}$ -BTC nanorod bundles. The growth of 1D nanocrystals is largely determined by the anisotropic nature of the Ln-BTC structure.

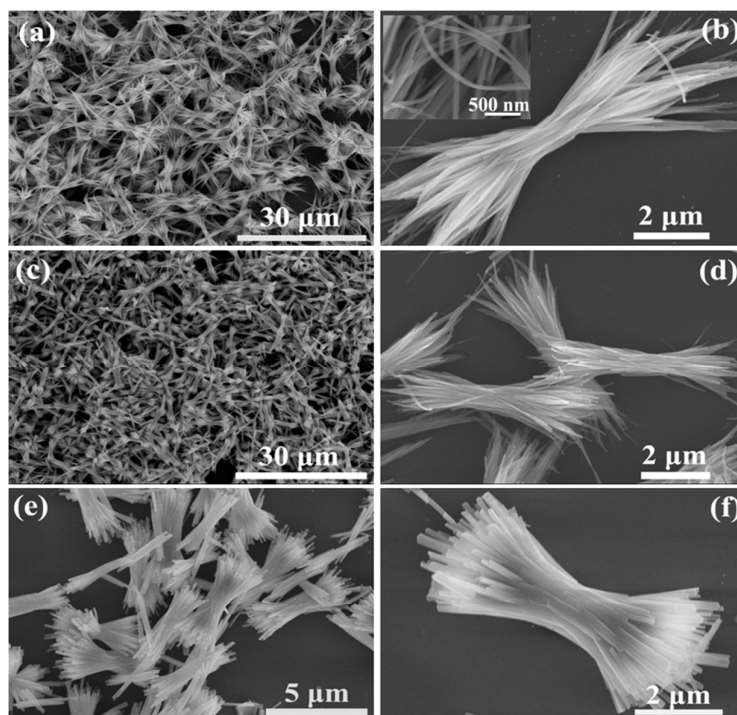


**Figure 4.** SEM images of the Ln-BTC 3D nanocrystalline architectures. (a, b) The obtained  $\text{Ce}_{0.90}\text{Eu}_{0.05}\text{Tb}_{0.05}$ -BTC 3D straw-sheaf structures. (c, d) The obtained Sm-BTC 3D straw-sheaf structures. Both of them are assembled by outspread and flexible nanobelts. (e, f) The



obtained Tm-BTC 3D straw-sheaf architectures, where the straw-sheaves are composed by rigid nanorods.

The morphology of the prepared nano-MOF was characterized by scanning electron microscopy (SEM). The low-magnification SEM images (Figure 3a) revealed that the  $Y_{0.95}Eu_{0.05}$ -BTC consist of a large quantity of well-dispersed 1D nanostructures with lengths of 20-50  $\mu\text{m}$ . The obvious creasing or curling places in the higher magnification SEM image (Figure 3b) provided evidence that the as-synthesized products are in a belt-like shape. It can be clearly seen that these nanobelts exhibit smooth surface, which are about 100-200 nm in width. The energy-dispersed X-ray spectroscopy (EDX) of the nanobelts shows several peaks corresponding to Y, Eu, C, and O elements in the range of 0–10 keV (Figure S3a), indicating that these nanobelts are formed from yttrium, europium, and benzenetricarboxylate, and the molar ratios of metal ions matched well with the assumed compound formula. Figures 3c and d give the  $Gd_{0.95}Eu_{0.05}$ -BTC products obtained at the same conditions. Instead of nanobelt formation, nanobundles appeared which are composed by several nanorods. The 1D nanorods exhibited smooth surface and rectangular cross section, without any creasing or curling places. They have widths of about 150-200 nm, thicknesses of  $\sim 50$  nm, and lengths of around several micrometers. Figure S2b shows the EDS spectrum of the final product, confirming that no elements other than C, O, Gd, and Eu present except the Si and Pt peaks from measurement. It is well-known that preferential growth often occurs in a crystal with structural anisotropy which has relatively small lateral adhesion energy.<sup>27</sup> In the present experiments, the formation of  $Y_{0.95}Eu_{0.05}$ -BTC nanobelts and  $Gd_{0.95}Eu_{0.05}$ -BTC nanorod bundles is largely determined by the anisotropic nature of the MOF structure. As shown in Figure 1b, one can see that the interesting feature of the compound is the presence of 1D ribbonlike molecular motif by coordinating interactions between the  $Ln^{3+}$  ion and BTC ligand. Thus, it suggests that the formed 1D ribbonlike structure could be responsible for the anisotropic nucleation and growth process of the 1D Ln-BTC nanostructures.

When BTC was reacted with other lanthanide ions ( $Sm^{3+}$ ,  $Tm^{3+}$ , and  $Ce^{3+}$ ), the morphology of these Ln(BTC) products changed to 3D nanoarchitectures assembled by 1D nanobelt or nanorod units. Figures 4a and 4b show typical SEM images of the uniform and well-dispersed straw-sheaflike  $Ce_{0.90}Eu_{0.05}Tb_{0.05}$ -BTC assemblies on a large scale. The product looks like straw-sheaf with two fantails consisting of a bundle of outspread and flexible nanobelts, which are closely bonded to each other in the middle, so it is called “straw-sheaf structure”. Careful observations revealed that the individual straw-sheaf has a length in the range of 7-10

$\mu\text{m}$  and a middle diameter in the range of 1-1.5  $\mu\text{m}$ . The prepared Sm-BTC also gave similar straw-sheaflike microstructures, as confirmed by Figures 4c and 4d. More interestingly, when the  $\text{Tm}^{3+}$  ions was mixed with BTC, the generated nano-MOF architectures are entirely composed of straw-sheaves with more obvious radiating fantails, as shown in Figures 4e and 4f. This morphology character is that a sheaf of rigid rodlike crystals have been bandaged in the middle, with the top and bottom fanning out while the middle remaining thin. The formation process of hierarchical architectures is a complex process, which is affected by both crystal growth environments and crystal structures, including the degree of super saturation, diffusion of the reaction, surface energy, crystal structures, and so forth.<sup>28</sup> The formation of these present hierarchical architectures is considered to be a crystal splitting process, as evidenced by some inorganic nanomaterials<sup>29,30</sup> and our previous results.<sup>23,24</sup>

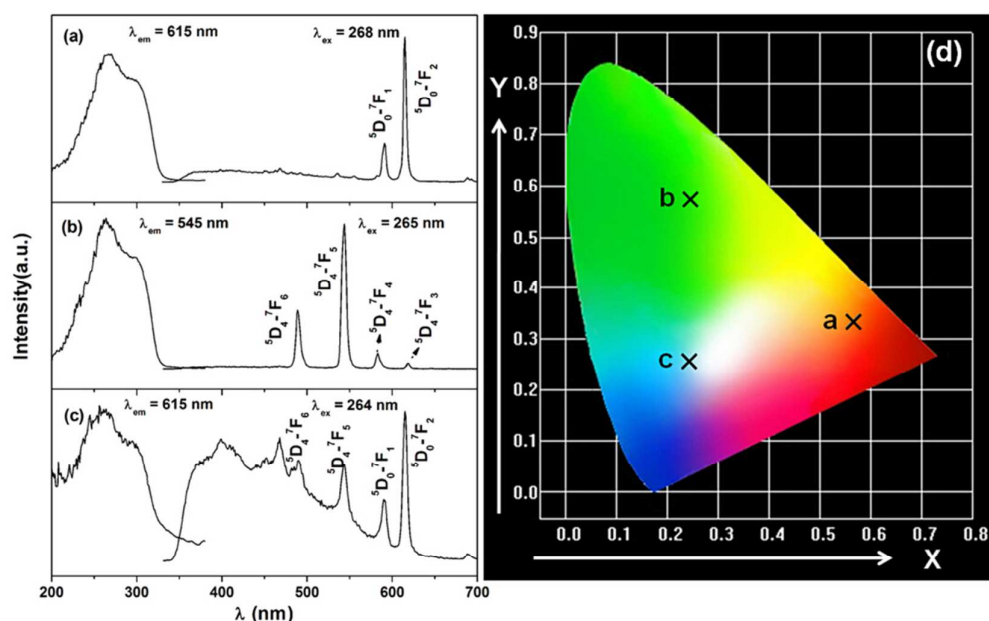


**Figure 5.** Photoluminescence properties of the as-prepared Ln-BTC nanocrystals. (a) Excitation and emission spectra of the  $\text{Gd}_{0.95}\text{Eu}_{0.05}$ -BTC nanorods, showing characteristic emissions of the  $\text{Eu}^{3+}$  ions. (b) Excitation and emission spectra of the  $\text{Gd}_{0.95}\text{Tb}_{0.05}$ -BTC nanorods, showing characteristic emissions of the  $\text{Tb}^{3+}$  ions. (c) Excitation and emission spectra of the  $\text{Ce}_{0.90}\text{Eu}_{0.05}\text{Tb}_{0.05}$ -BTC nanoarchitectures. The co-existed blue, green, and red emissions approach white-light region, indicating the partial energy transfer from the BTC ligand to  $\text{Eu}^{3+}$  and  $\text{Tb}^{3+}$  ions. (d) CIE chromaticity diagram for the  $\text{Gd}_{0.95}\text{Eu}_{0.05}$ -BTC (a point 0.565, 0.334),  $\text{Gd}_{0.95}\text{Tb}_{0.05}$ -BTC (b point, 0.245, 0.572), and  $\text{Ce}_{0.90}\text{Eu}_{0.05}\text{Tb}_{0.05}$ -BTC (c point

0.243, 0.256), confirming the tunable photoluminescence by doping or codoping  $\text{Eu}^{3+}$  and  $\text{Tb}^{3+}$  ions.

The photoluminescence properties of Ln-BTC assemblies were investigated in detail. Figure 5a shows the excitation and emission spectra of the  $\text{Gd}_{0.95}\text{Eu}_{0.05}$ -BTC nanorods. The excitation broadband with two maximum at 260 and 292 nm are due to the charge-transfer band between the  $\text{O}^{2-}$  and  $\text{Eu}^{3+}$  ions and  $\pi$ - $\pi^*$  electron transition of the organic bridging ligand, respectively.<sup>22,31</sup> On excitation at 268 nm, the emission spectrum consists of two main peaks at about 589 and 615 nm, which are assigned to the  $^5\text{D}_0$ - $^7\text{F}_1$  and  $^5\text{D}_0$ - $^7\text{F}_2$  transitions of the  $\text{Eu}^{3+}$  ions, respectively. This result indicates that the  $\text{Eu}^{3+}$  ions are essentially excited by host Gd-BTC absorption. When the  $\text{Tb}^{3+}$  ions was doped into the same host, the excitation is similar while the emission exhibits four peaks centered at 489, 544, 585, and 620 nm, which correspond to the  $^5\text{D}_4$ - $^7\text{F}_J$  ( $J = 6, 5, 4$  and  $3$ ) transitions of the  $\text{Tb}^{3+}$  ions, respectively (Figure 5b). Furthermore, the  $\text{Y}_{0.95}\text{Eu}_{0.05}$ -BTC nanobelts exhibited characteristic emission of the  $\text{Eu}^{3+}$  ions (Figure S3). These results indicated that the efficient energy transfer from the nano-MOF Ln-BTC host to the doped  $\text{Eu}^{3+}$  and  $\text{Tb}^{3+}$  ions. However, the emission spectra of the  $\text{Ce}_{0.90}\text{Eu}_{0.05}\text{Tb}_{0.05}$ -BTC sample excited at 264 nm exhibited not only the characteristic emissions of the  $\text{Eu}^{3+}$  and  $\text{Tb}^{3+}$  ions, but also the blue emission of BTC ligand (Figure 5c). The stronger broadband in the range from 350 to 550nm comes from the emission of the BTC in the  $\text{Ce}_{0.90}\text{Eu}_{0.05}\text{Tb}_{0.05}$ -BTC, revealing that the partial efficient energy transfer takes place from BTC to doped  $\text{Eu}^{3+}$  and  $\text{Tb}^{3+}$  ions, compare with the emission spectra of the  $\text{Gd}_{0.95}\text{Eu}_{0.05}$ -BTC,  $\text{Gd}_{0.95}\text{Tb}_{0.05}$ -BTC and  $\text{Y}_{0.95}\text{Eu}_{0.05}$ -BTC, where very weak emission can be observed. Very interestingly, white-light emission can be approached in the present system, as confirmed by the CIE chromaticity diagram (Figure 5d).

#### 4. Conclusions

A series of nano/micro-sized lanthanide-based metal-organic frameworks have been developed via a simple, rapid, and effective one-step method. 1D nanostructures and 3D assembled nanoarchitectures can be obtained by using different lanthanide ions to chelate benzenetricarboxylic acid. The different forms of splitting are in accordance with the anisotropic crystal structure of the Ln-BTC. The as-prepared samples show tunable emissions between red and green due to the efficient energy transfer from BTC to doped  $\text{Eu}^{3+}$  and  $\text{Tb}^{3+}$  ions. Interestingly, white-light emission from  $\text{Ce}_{0.90}\text{Eu}_{0.05}\text{Tb}_{0.05}$ -BTC nano-MOF can be

approached via limiting energy transfer. We believe that the present results may serve as a guidance for the design and fabrication of novel MOF nanomaterials in a simple way.

### Acknowledgments

This work is financially supported by the natural science foundation of Shandong Province (Grant No. 20771098) and Higher Educational Science and Technology Program of Shandong Province, China (Grant No. J13LD11).

### Reference

1. (a) O. M. Yaghi, M. Obkeeffe, N. W. Ockwig, H. K. Chae, M. Eddaoudi and J. Kim, *Nature*, 2003, **423**, 705; (b) X. Zhao, B. Xiao, A. J. Fletcher, K. M. Thomas, D. Bradshaw and M. J. Rosseinsky, *Science*, 2004, **306**, 1012.
2. J. S. Seo, D. Whang, H. Lee, S. I. Jun, J. Oh, Y. J. Jeon and K. Kim, *Nature*, 2000, **404**, 982.
3. O. R. Evans and W. Lin, *Acc. Chem. Res.*, 2002, **35**, 511.
4. (a) F. M. Tabellion, S. R. Seidel, A. M. Arif and P. J. Stang, *J. Am. Chem. Soc.*, 2001, **123**, 7740; (b) M. E. Kosal, J.-H. Chou, S. R. Wilson and K. S. Suslick, *Nat. Mater.*, 2002, **1**, 118.
5. (a) O. Moonhyun and C. A. Mirkin, *Nature*, 2005, **438**, 651; (b) Y. M. Jeon, G. S. Armatas, D. Kim, M. G. Kanatzidis and C. A. Mirkin, *Small*, 2009, **5**, 46.
6. K. M. L. Taylor, W. J. Rieter and W. Lin, *J. Am. Chem. Soc.*, 2008, **130**, 14358.
7. Y. H. Wang, B. Li, Y. H. Liu, L. M. Zhang, Q. H. Zuo, L. F. Shi and Z. M. Su, *Chem. Commun.*, **2009**, 5868.
8. K. M. L. Taylor, A. Jin and W. Lin, *Angew. Chem., Int. Ed.*, 2008, **47**, 7722.
- 9 (a) H. J. Lee, W. Cho, S. Jung and M. Oh, *Adv. Mater.*, 2009, **21**, 674; (b) S. Jung, W. Cho, H. J. Lee and M. Oh, *Angew. Chem., Int. Ed.*, 2009, **48**, 1459.
10. R.C. Huxford-Phillips, S.R. Russell, D. Liu, and W. Lin, *RSC Adv.* 2013, **3**, 14438.
11. K. E. deKrafft, W.S. Boyle, L.M. Burk, O.Z. Zhou, and W. Lin, *J. Mater. Chem.* 2012, **35**, 18065.
13. J. Della Rocca, D. Liu, and W. Lin, *Acc. Chem. Res.* 2011, **44**, 957.
14. H. Guo, Y. Zhu, S. Qiu, J. A. Lercher, and H. Zhang, *Adv. Mater.* 2010, **22**, 4190.
15. M. Jahan, Q. Bao, J. Yang, and K. P. Loh, *J. Am. Chem. Soc.*, 2008, **132**, 14487.
16. (a) W. S. Liu, T. Q. Jiao, Y. Z. Li, Q. Z. Liu, M. Y. Tan, H. Wang, and L. F. Wang, *J. Am. Chem. Soc.* 2004, **126**, 2280. (b) C. Serre, N. Stock, T. Bein, and G. Ferey, *Inorg. Chem.* 2004, **43**, 3159.

17. (a) G. Mancino, A. J. Ferguson, A. Beeby, N. J. Long, and T.S. Jones, *J. Am. Chem. Soc.* 2005, **127**, 524. (b) L. D. Carlos, R. A. S. Ferreira, V. Bermudez, and S. J. L. Ribeiro, *Adv. Mater.* 2009, **21**, 509.
18. T. M. Reineke, M. Eddaoudi, M. O'Keeffe, and O. M. Yaghi, *Angew. Chem., Int. Ed.* 1999, **38**, 2590.
19. (a) B. L. Chen, Y. Yang, F. Zapata, G. N. Lin, G. D. Qian, and E. B. Lobkovsky, *Adv. Mater.* 2007, **19**, 1693. (b) B. L. Chen, L. B. Wang, F. Zapata, G. D. Qian, and E. B. Lobkovsky, *J. Am. Chem. Soc.* 2008, **130**, 6718.
20. X. D. Guo, G. S. Zhu, Z. Y. Li, F. X. Sun, Z. H. Yang, and S. L. Qiu, *Chem. Commun.* 2006, 3172. (b) X. D. Guo, G. S. Zhu, Z.Y. Li, Y. Chen, X. T. Li, and S. L. Qiu, *Inorg. Chem.* 2006, **45**, 4065. (c) Z.Y. Li, G. S. Zhu, X. D. Guo, X. J. Zhao, Z. Jin, and S. L. Qiu, *Inorg. Chem.* 2007, **45**, 5174.
21. Y. Cui, B. Chen, and G. Qian, *Coord. Chem. Rev.*, 2014, **273-274**, 76.
22. K. Liu, H. P. You, G. Jia, Y. H. Zheng, Y. H. Song, M. Yang, Y. J. Huang, and H. J. Zhang, *Cryst. Growth Des.* 2009, **9**, 3519.
23. K. Liu, H. P. You, Y. H. Zheng, G. Jia, L. H. Zhang, Y. J. Huang, M. Yang, Y. H. Song, and H. J. Zhang, *CrystEngComm.* 2009, **11**, 2622.
24. K. Liu, H. P. You, Y. H. Zheng, G. Jia, Y. Huang, M. Yang, Y. H. Song, L. H. Zhang, and H. J. Zhang, *Cryst. Growth Des.* 2010, **10**, 16.
25. K. Liu, H. P. You, Y. H. Zheng, G. Jia, Y. H. Song, Y. J. Huang, M. Yang, J. J. Jia, N. Guo, and H. J. Zhang, *J. Mater. Chem.* 2010, **32**, 3272.
26. Y. H. Wen, J. K. Cheng, Y. L. Feng, J. Zhang, Z. J. Li, and Y. G. Yao, *Chin. J. Struct. Chem.* 2005, **12**, 1440.
27. (a) S. M. Lee, S. N. Cho and J. Cheon, *Adv. Mater.*, 2003, **15**, 441; (b) J. P. Liu, Y. Y. Li, X. T. Huang, Z. K. Li, G. Y. Li and H. B. Zeng, *Chem. Mater.*, 2008, **20**, 250; (c) W. M. Du, J. Zhu, S. X. Li and X. F. Qian, *Cryst. Growth Des.*, 2008, **8**, 2130.
28. (a) L. S. Zhong, J. S. Hu, H. P. Liang, A. M. Cao, W. G. Song, and L. J. Wan, *Adv. Mater.* 2006, **18**, 2426. (b) Z. P. Zhang, X. Q. Shao, H. D. Yu, Y. B. Wang, and M. Y. Han, *Chem. Mater.* 2005, **17**, 332.
29. J. Tang, and A. P. Alivisatos, *Nano Lett.* 2006, **6**, 2701.
30. H. Deng, C. M. Liu, S. H. Yang, S. Xiao, Z. K. Zhou, and Q. Q. Wang, *Cryst. Growth Des.* 2008, **8**, 4432.
31. Y. S. Yang, M. L. Gong, and Y. Y. Li, *J. Alloys Compd.* 1994, **207-208**, 112.